SUPPLEMENTARY INFORMATION

Boron-Based Ternary $MgTa_2B_6$ Cluster: A Turning Nanoclock with Dynamic Structural Fluxionality

Fang-Lin Liu, Jin-Chang Guo, and Hua-Jin Zhai*

Nanocluster Laboratory, Institute of Molecular Science, Shanxi University, Taiyuan 030006, China

*E-mail: hj.zhai@sxu.edu.cn

Supplementary Information – Part I

Table S1 Cartesian coordinates for optimized global-minimum (GM) and transition-state (TS) structures of $MgTa_2B_6$ cluster at the PBE0-D3BJ/def2-TZVP level.

Table S2 Orbital composition analysis for occupied canonical molecular orbitals (CMOs) of GM (**1**, C_s, $^1A'$) $MgTa_2B_6$ cluster. Main components are highlighted in bold.

Table S3 Orbital composition analysis for occupied CMOs of TS (**1′**, C_s, $^1A'$) $MgTa_2B_6$ cluster. Main components are highlighted in bold.

Table S4 Calculated $NICS_{zz}$ and NICS (shown in *italics* in brackets) of GM (**1**, C_s, $^1A'$) $MgTa_2B_6$ cluster at the PBE0/Ta/def2-TZVP/B,Mg/6-311+G(d) level. These values are calculated at the center of B_6 ring or B_4 trapezoid, as well as at 1 Å above the center.

Figure S1 Optimized geometric structures for the top 20 low-lying isomers of $MgTa_2B_6$ cluster at the PBE0-D3BJ/def2-TZVP level along with their relative energies (in

italics), including corrections for the zero-point energies (ZPEs). Relative energies are also listed at the single-point CCSD(T)/def2-TZVP//PBE0-D3BJ/def2-TZVP level with ZPE corrections, as well as at the single-point CCSD(T)/def2-TZVP//BP86-D3BJ/def2-TZVP level (in brackets) with ZPE corrections. All energies are shown in kcal mol^{-1}.

Figure S2 Calculated bond distances (in Å; black color) and Wiberg bond indices (WBIs; in blue color) for GM $MgTa_2B_6$ cluster at the PBE0-D3BJ/def2-TZVP level. The WBI values are obtained from the natural bond orbital (NBO) analysis.

Figure S3 Calculated (a) bond distances (in Å; black color) and (b) WBIs (blue color) for TS $MgTa_2B_6$ cluster. The WBIs are obtained from the NBO analysis.

Figure S4 Pictures of occupied CMOs of GM (**1**, C_s, $^1A'$) $MgTa_2B_6$ cluster, sorted to five subsets. (a) Six CMOs for skeleton, localized B–B σ bonds along the peripheral B_6 ring. (b) Three delocalized π CMOs; that is, the π sextet. (c) Three delocalized σ CMOs. (d) Two Ta 5d-based CMOs that are approximately Ta–Ta nonbonding, with secondary d-p σ bonding. (e) One σ bond within the Ta8–Mg9 unit (see Fig. 1(a) for atom labels), as well as the lowest unoccupied molecular orbital (LUMO). Subsets (b) and (c) collectively render the $MgTa_2B_6$ cluster 6π/6σ double aromaticity.

Figure S5 Calculated natural atomic charges (in |e|) of a model D_{6h} CB_6^{2-} cluster from the NBO analysis at the PBE0-D3BJ/def2-TZVP level.

Figure S6 An alternative chemical bonding scheme for GM (**1**, C_s, $^1A'$) $MgTa_2B_6$ cluster on the basis of adaptive natural density partitioning (AdNDP) analysis. Occupation numbers (ONs) are indicated.

Figure S7 Isosurfaces of electron localization functions (ELFs) for GM $MgTa_2B_6$ cluster. (a) At the B_6 plane. (b) At the plane of B3–Ta8–B6–Ta7 rhombus.

Figure S8 Pictures of occupied CMOs of TS (**1′**, C_s, $^1A'$) structure of $MgTa_2B_6$ cluster. (a) Six CMOs for localized B–B σ bonds along the peripheral B_6 ring. (b) Three

delocalized π CMOs. (c) Three delocalized σ CMOs. (d) Two Ta 5d-based CMOs that are approximately Ta−Ta nonbonding. (e) One σ bond within the Ta8−Mg9 unit, as well as the LUMO.

Figure S9 AdNDP bonding scheme for the TS structure of $MgTa_2B_6$ cluster. The ONs are shown. This bonding scheme is to be compared to that of GM $MgTa_2B_6$ cluster as shown in Fig. 4.

Supplementary Information – Part II

A short movie extracted from the Born-Oppenheimer molecular dynamics (BOMD) simulation for GM $MgTa_2B_6$ cluster. The simulation was performed at near room temperature (300 K) for a time duration of 60 ps. The movie roughly covers a time span of 12 ps.

Table S1 Cartesian coordinates for optimized global-minimum (GM) and transition-state (TS) structures of $MgTa_2B_6$ cluster at the PBE0-D3BJ/def2-TZVP level.

1 (GM, C_s, $^1A'$)

B	0.79142705	1.39983409	0.00265237
B	-0.82052483	1.38297912	0.00265237
B	-1.59640516	-0.01904227	0.00592409
B	-0.78469099	-1.39741379	-0.00857646
B	0.81373964	-1.38070020	-0.00857646
B	1.59645430	0.01434306	0.00592409
Ta	0.00001937	-0.00185289	-1.47094945
Ta	0.00001937	-0.00185289	1.51355369
Mg	-0.02720039	2.60135261	2.67545797

1′ (TS, C_s, $^1A'$)

B	0.01759854	1.61053394	-0.00964987
B	-1.38027195	0.81283623	0.00512060
B	-1.39059116	-0.78526101	-0.01234223
B	-0.01753949	-1.60512975	0.02409312
B	1.37309985	-0.81546027	-0.01234223
B	1.39770421	0.78248087	0.00512060
Ta	0.00000293	0.00026830	1.47148794
Ta	0.00000293	0.00026830	-1.51217717
Mg	0.02827561	2.58764807	-2.74741123

Table S2 Orbital composition analysis for occupied canonical molecular orbitals (CMOs) of GM (**1**, C_s, ^{1}A′) $MgTa_2B_6$ cluster. Main components are highlighted in bold.

Subsystem	CMO	B_6 (%)		Ta_2 (%)		Mg (%)	
		s/p	total	s/p/d	total	s/p	total
B–B 2c-2e σ	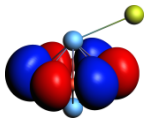 HOMO−7 (a′)	0.2/**96.7**	**96.9**	0.0/0.1/0.4	0.5	0.2/0.0	0.2
	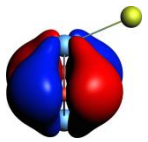 HOMO−10 (a″)	**23.4/54.9**	**78.3**	0.0/0.0/19.8	19.8	0.0/0.0	0.0
	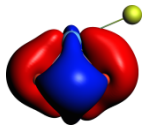 HOMO−11 (a′)	**22.7/54.9**	**77.6**	0.1/0.2/**20.0**	**20.3**	0.3/0.0	0.3
	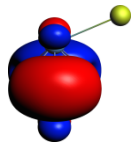 HOMO−12 (a″)	**36.0/27.7**	**63.7**	0.0/4.6/**25.5**	**30.1**	0.0/0.0	0.0
	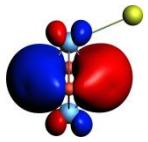 HOMO−13 (a′)	**36.0/27.6**	**63.6**	0.0/4.8/**25.3**	**30.1**	0.1/0.1	0.2
	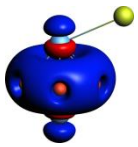 HOMO−14 (a′)	**48.5**/18.6	**67.1**	7.3/5.6/4.1	17.0	0.2/0.1	0.3
Mg–Ta 2c-2e σ	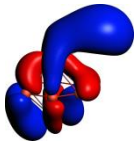 HOMO (a′)	2.0/**22.2**	**24.2**	3.9/5.4/**32.5**	**41.8**	**30.3**/1.9	**32.2**

6π aromaticity	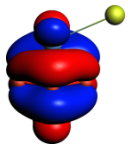 HOMO−5 (a″)	0.1/**60.7**	**60.8**	0.0/2.2/**34.5**	**36.7**	0.0/0.1	0.1
	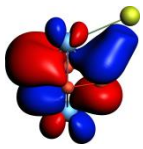 HOMO−6 (a′)	1.7/**59.1**	**60.8**	0.3/3.8/**27.0**	**31.1**	5.3/0.1	5.4
	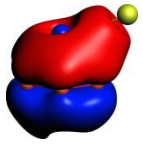 HOMO−9 (a′)	0.6/**67.5**	**68.1**	12.6/2.5/6.5	**21.6**	3.9/0.1	4.0
6σ aromaticity	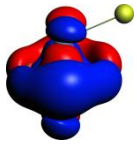 HOMO−3 (a″)	16.2/**55.0**	**71.2**	0.0/6.7/**20.1**	**26.8**	0.0/0.3	0.3
	 HOMO−4 (a′)	8.2/**36.0**	**44.2**	1.0/6.1/**28.8**	**35.9**	17.9/0.0	17.9
	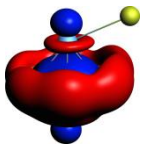 HOMO−8 (a′)	**23.7/36.8**	**60.5**	1.7/0.2/**34.2**	**36.1**	1.0/0.0	1.0
Ta d-based CMOs	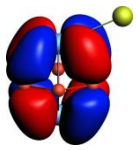 HOMO−1 (a″)	0.2/**28.7**	**28.9**	0.0/0.1/**70.2**	**70.3**	0.0/0.2	0.2
	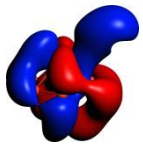 HOMO−2 (a′)	5.7/**35.3**	**41.0**	1.2/2.5/**45.3**	**49.0**	8.3/0.4	8.7

Table S3 Orbital composition analysis for occupied CMOs of TS (**1′**, C_s, ^{1}A′) $MgTa_2B_6$ cluster. Main components are highlighted in bold.

Subsystem	CMO	B_6 (%)		Ta_2 (%)		Mg (%)	
		s/p	total	s/p/d	total	s/p	total
B–B 2c-2e σ	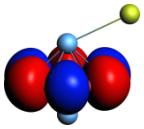 HOMO−7 (a″)	0.0/**97.7**	**97.7**	0.0/0.0/0.1	0.1	0.0/0.0	0.0
	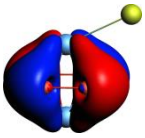 HOMO−10 (a″)	**23.2/55.2**	**78.4**	0.0/0.0/19.7	19.7	0.0/0.0	0.0
	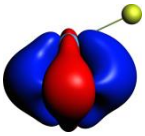 HOMO−11 (a′)	**23.2/54.4**	**77.6**	0.1/0.1/**20.2**	**20.4**	0.2/0.0	0.2
	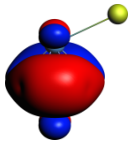 HOMO−12 (a″)	**36.0/27.7**	**63.7**	0.0/4.6/**25.5**	**30.1**	0.0/0.0	0.0
	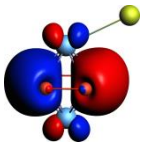 HOMO−13 (a′)	**36.1/27.5**	**63.6**	0.0/4.7/**25.4**	**30.1**	0.1/0.1	0.2
	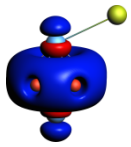 HOMO−14 (a′)	**48.5**/18.6	**67.1**	7.3/5.6/4.1	17.0	0.2/0.1	0.3
Mg–Ta 2c-2e σ	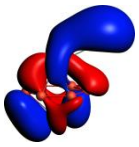 HOMO (a′)	2.0/**23.1**	**25.1**	3.5/5.0/**35.3**	**43.8**	**27.8**/1.6	**29.4**

6π aromaticity	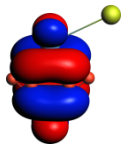 HOMO−5 (a″)	0.1/**60.6**	**60.7**	0.0/2.1/**34.6**	**36.7**	0.0/0.1	0.1
	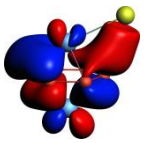 HOMO−6 (a′)	2.2/**57.5**	**59.7**	0.4/4.3/**25.6**	**30.3**	7.2/0.0	7.2
	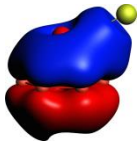 HOMO−9 (a′)	0.5/**67.4**	**67.9**	12.7/2.6/6.3	**21.6**	4.0/0.1	4.1
6σ aromaticity	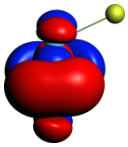 HOMO−3 (a″)	16.1/**55.1**	**71.2**	0.0/6.7/**20.2**	**26.9**	0.0/0.3	0.3
	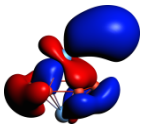 HOMO−4 (a′)	7.3/**35.3**	**42.6**	1.1/5.7/**30.2**	**37.0**	18.3/0.0	18.3
	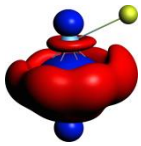 HOMO−8 (a′)	**23.8/36.5**	**60.3**	1.7/0.2/**34.5**	**36.4**	0.9/0.0	0.9
Ta d-based CMOs	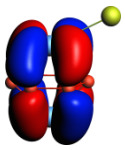 HOMO−1 (a″)	0.2/**28.0**	**28.2**	0.0/0.1/**71.0**	**71.1**	0.0/0.2	0.2
	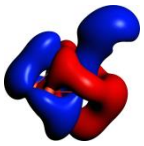 HOMO−2 (a′)	6.3/**36.7**	**43.0**	1.3/2.8/**42.0**	**46.1**	9.2/0.4	9.6

Table S4 Calculated $NICS_{zz}$ and NICS (shown in *italics* in brackets) of GM (**1**, C_s, $^1A'$) $MgTa_2B_6$ cluster at the PBE0/Ta/def2-TZVP/B,Mg/6-311+G(d) level. These values are calculated at the center of B_6 ring or B_4 trapezoid, as well as at 1 Å above the center.

R (Å)	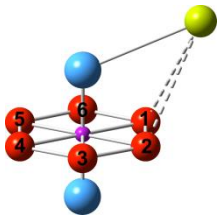 B_6 ring	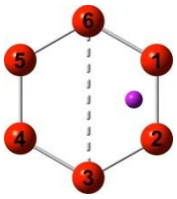 B_4 trapezoid	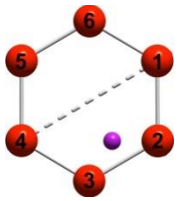 B_4 trapezoid	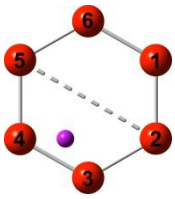 B_4 trapezoid	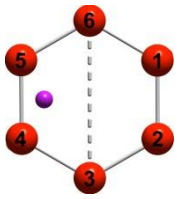 B_4 trapezoid
0.0	–91.43 (*–100.03*)	–77.20 (*–54.11*)	–74.01 (*–52.78*)	–67.00 (*–49.28*)	–64.77 (*–46.68*[a])
1.0	–141.14 (+57.84[b])	–59.94 (+5.11[b])	–52.62 (+7.73[b])	–39.08 (+10.35[b])	–36.18 (+9.51[b])

[a] The dissected contributions from a subset of CMOs to the total NICS value can be evaluated using the NBO 6.0 package. As an example, we shall analyze a point located 0.5 Å below the center of B3B4B5B6 trapezoid. Here the total NICS value is highly negative (–39.62 ppm), to which the delocalized 6π and 6σ frameworks (Fig. S4(b) and S4(c)) contribute by 74.5% collectively. To be specific, the three delocalized σ CMOs have a contribution of –19.54 ppm, as compared to –10.03 ppm from three delocalized π CMOs. In other words, the delocalized σ and π CMOs account for 49.2% and 25.3% of the total NICS value, respectively. Note that these numbers are merely an example. This analysis further validates the concept of double π/σ aromaticity in the ternary cluster.

[b] These NICS(1) values are not a very reliable indicator of π aromaticity, due to the perturbation of a Ta atom in the vicinity. The Ta atom is 1.49 Å above/below the B_6 plane.

Figure S1 Optimized geometric structures for the top 20 low-lying isomers of $MgTa_2B_6$ cluster at the PBE0-D3BJ/def2-TZVP level along with their relative energies (in *italics*), including corrections for the zero-point energies (ZPEs). Relative energies are also listed at the single-point CCSD(T)/def2-TZVP//PBE0-D3BJ/def2-TZVP level with ZPE corrections, as well as at the single-point CCSD(T)/def2-TZVP//BP86-D3BJ/def2-TZVP level (in brackets) with ZPE corrections. All energies are shown in kcal mol^{-1}.

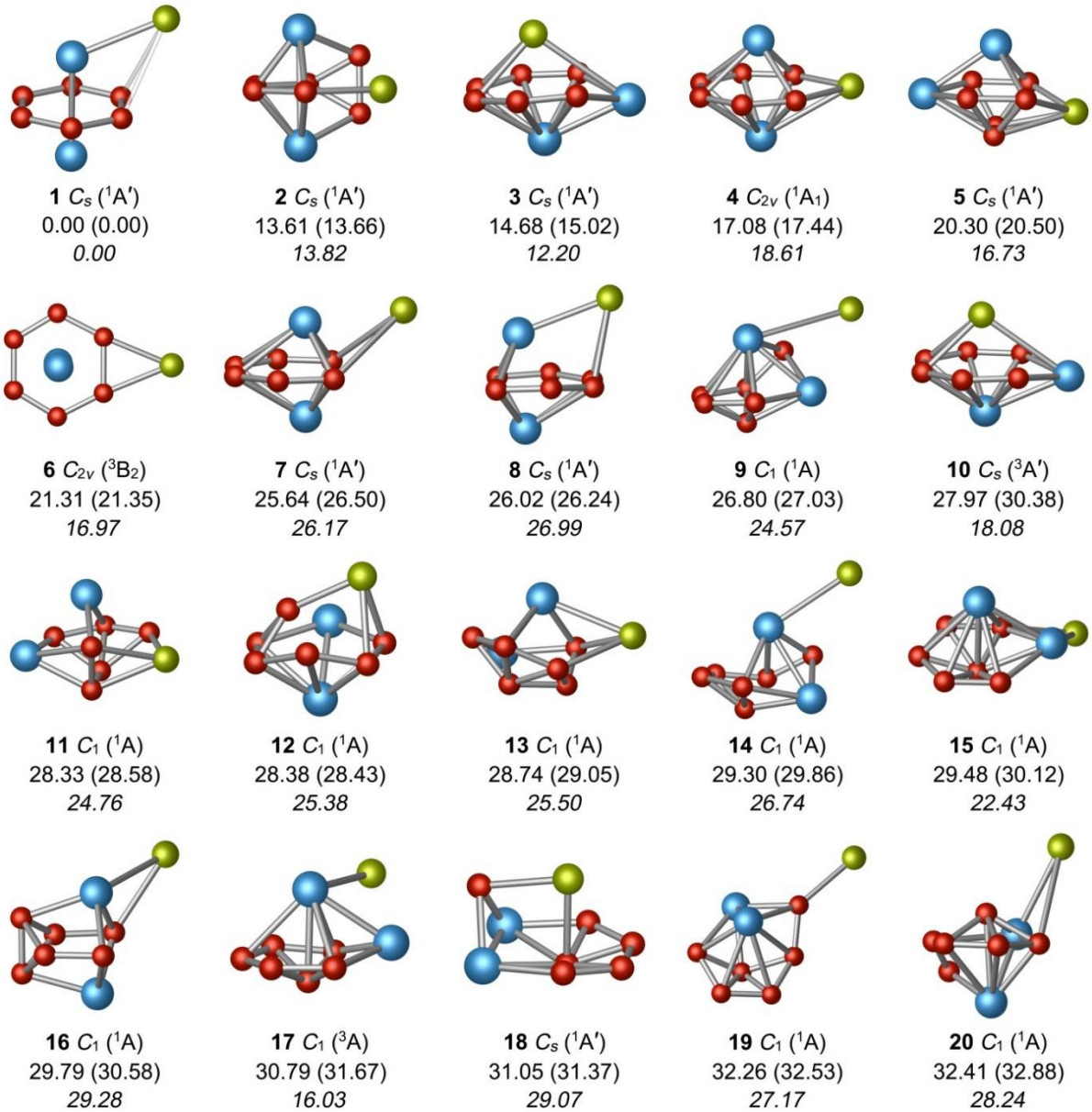

Figure S2 Calculated bond distances (in Å; black color) and Wiberg bond indices (WBIs; in blue color) for GM $MgTa_2B_6$ cluster at the PBE0-D3BJ/def2-TZVP level. The WBI values are obtained from the natural bond orbital (NBO) analysis.

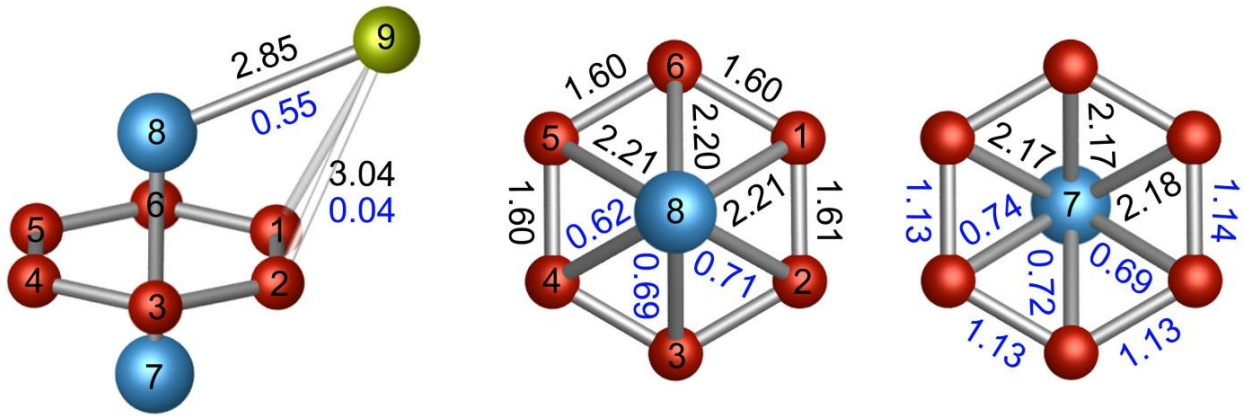

Figure S3 Calculated (a) bond distances (in Å; black color) and (b) WBIs (blue color) for TS $MgTa_2B_6$ cluster. The WBIs are obtained from the NBO analysis.

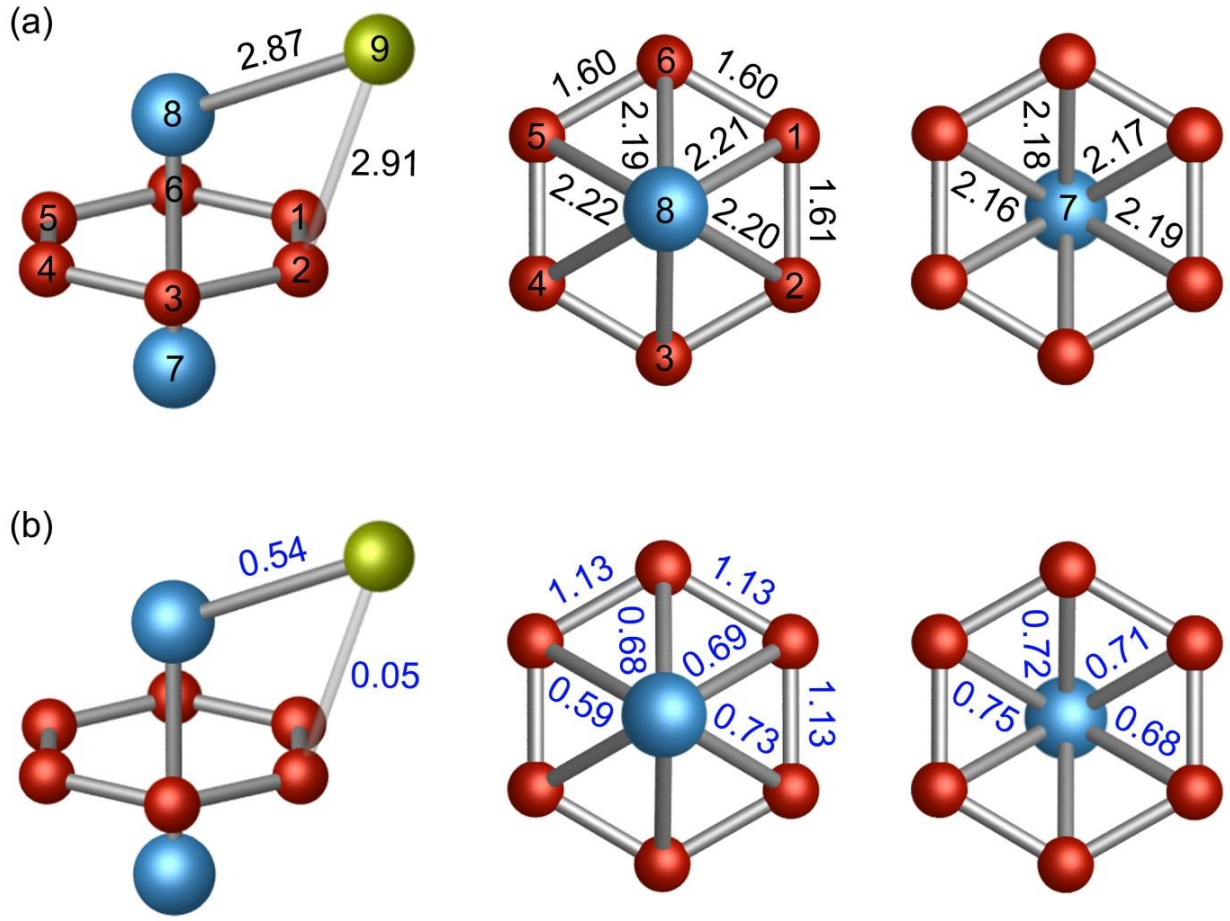

Figure S4 Pictures of occupied CMOs of GM (**1**, C_s, $^1A'$) $MgTa_2B_6$ cluster, sorted to five subsets. (a) Six CMOs for skeleton, localized B–B σ bonds along the peripheral B_6 ring. (b) Three delocalized π CMOs; that is, the π sextet. (c) Three delocalized σ CMOs. (d) Two Ta 5d-based CMOs that are approximately Ta–Ta nonbonding, with secondary d-p σ bonding. (e) One σ bond within the Ta8–Mg9 unit (see Fig. 1(a) for atom labels), as well as the lowest unoccupied molecular orbital (LUMO). Subsets (b) and (c) collectively render the $MgTa_2B_6$ cluster 6π/6σ double aromaticity.

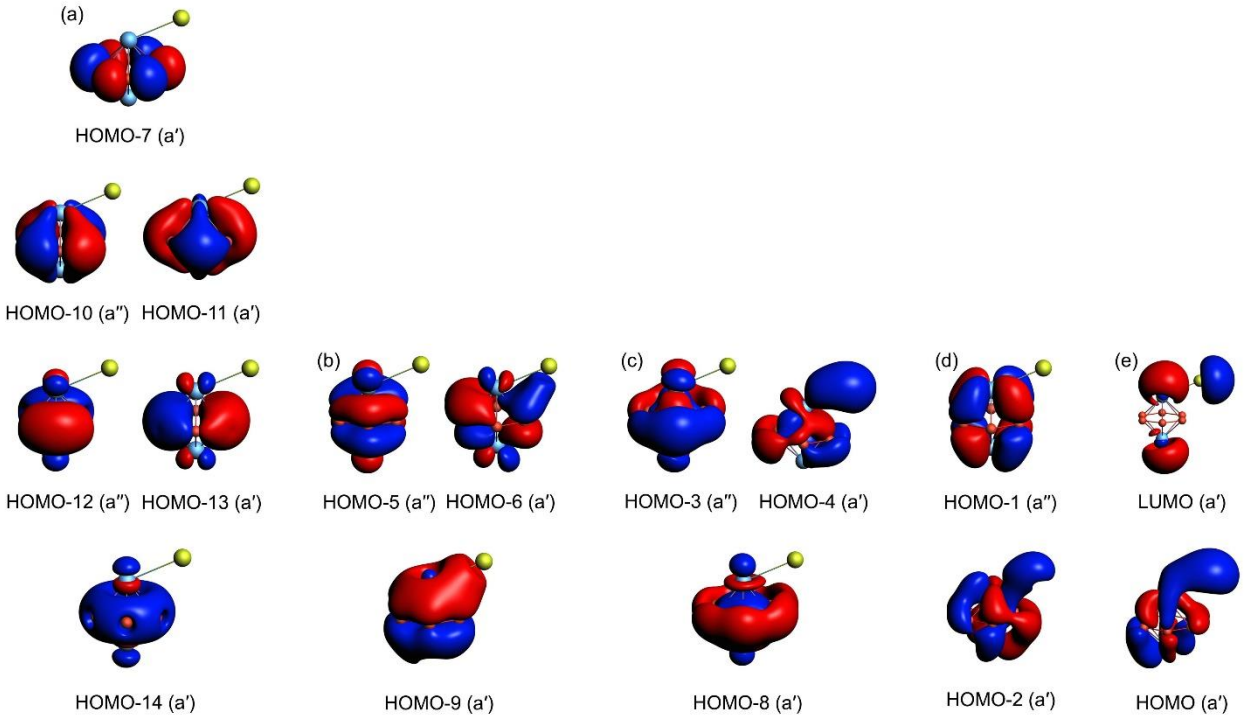

Figure S5 Calculated natural atomic charges (in |e|) of a model D_{6h} CB_6^{2-} cluster from the NBO analysis at the PBE0-D3BJ/def2-TZVP level.

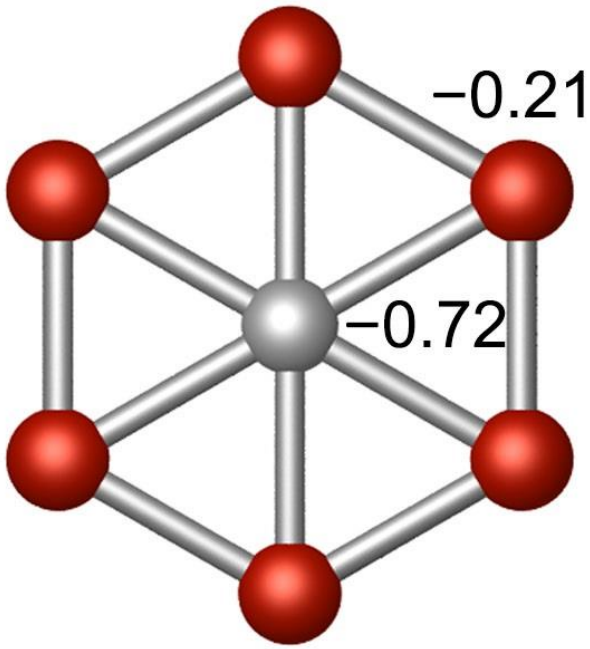

CB_6^{2-} (D_{6h})

Figure S6 An alternative chemical bonding scheme for GM (**1**, C_s, $^1A'$) $MgTa_2B_6$ cluster on the basis of adaptive natural density partitioning (AdNDP) analysis. Occupation numbers (ONs) are indicated.

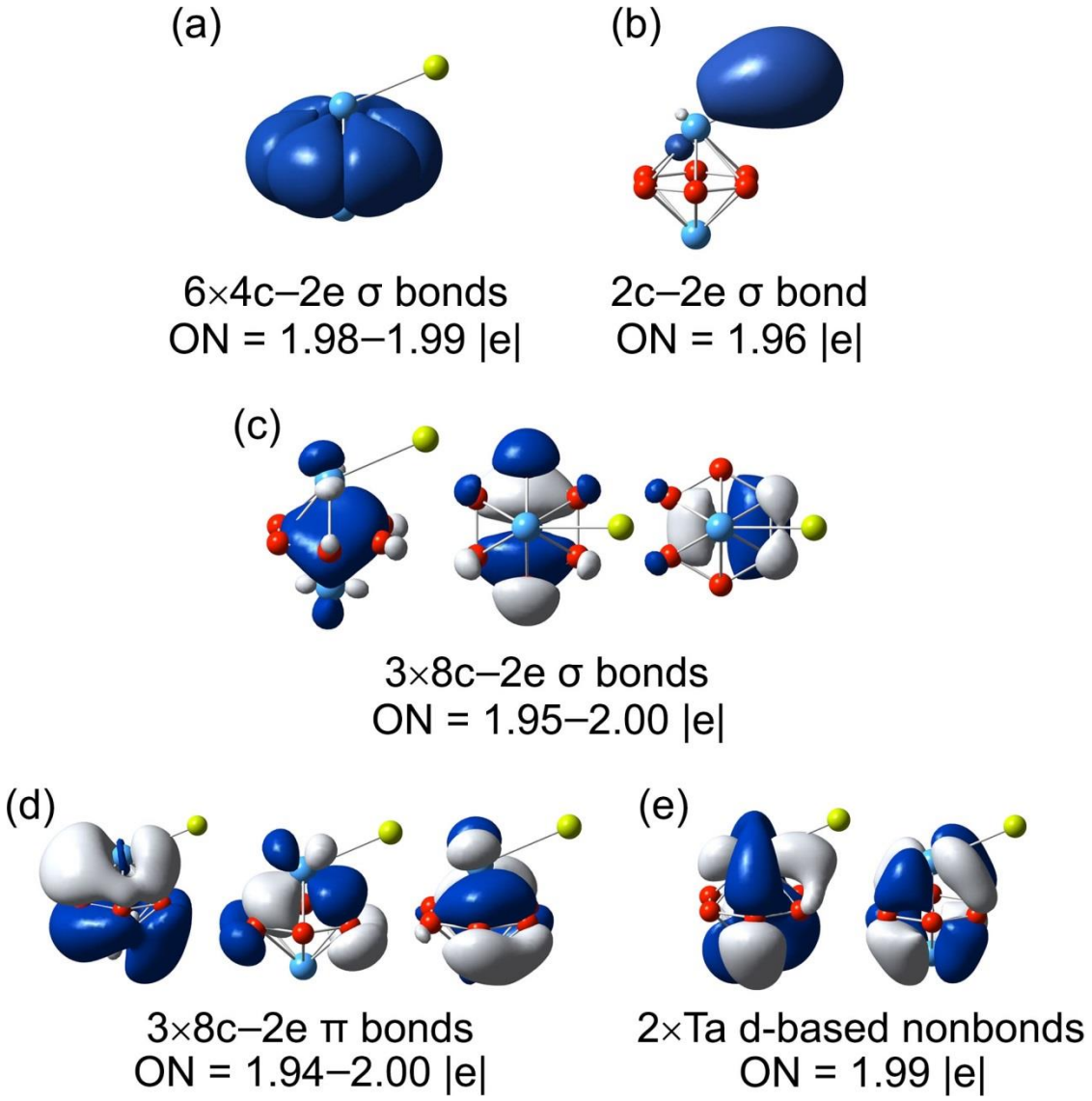

Figure S7 Isosurfaces of electron localization functions (ELFs) for GM $MgTa_2B_6$ cluster. (a) At the B_6 plane. (b) At the plane of B3–Ta8–B6–Ta7 rhombus.

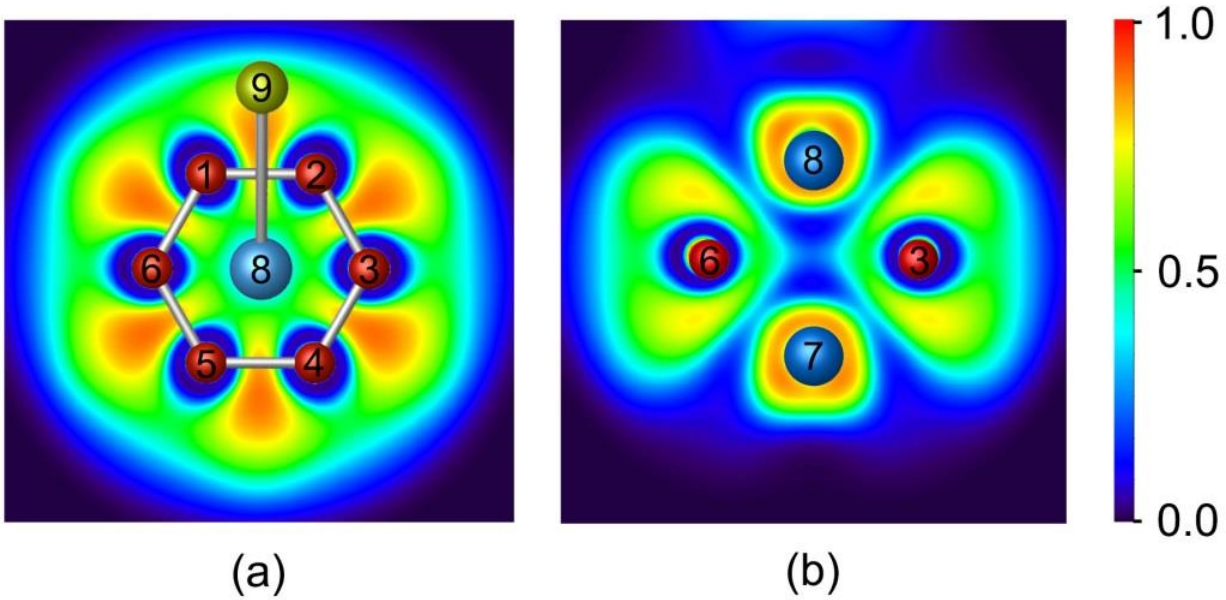

Figure S8 Pictures of occupied CMOs of TS (**1′**, C_s, $^1A'$) structure of $MgTa_2B_6$ cluster. (a) Six CMOs for localized B–B σ bonds along the peripheral B_6 ring. (b) Three delocalized π CMOs. (c) Three delocalized σ CMOs. (d) Two Ta 5d-based CMOs that are approximately Ta–Ta nonbonding. (e) One σ bond within the Ta8–Mg9 unit, as well as the LUMO.

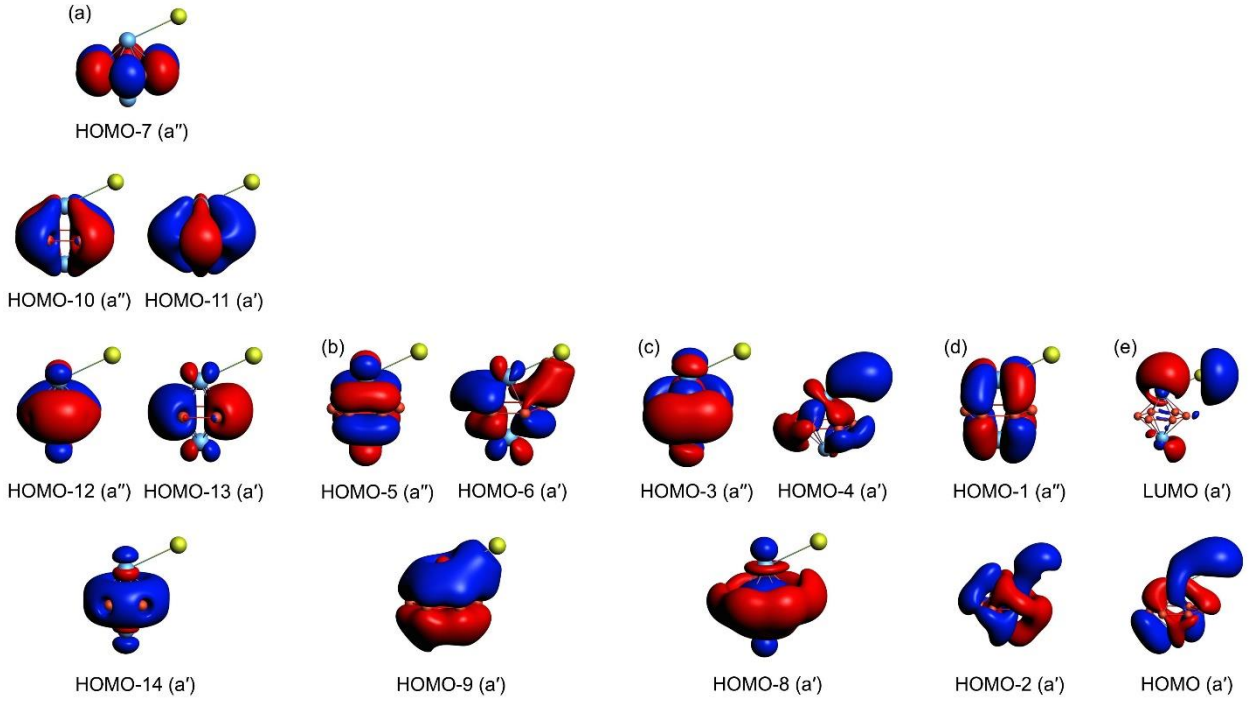

Figure S9 AdNDP bonding scheme for the TS structure of $MgTa_2B_6$ cluster. The ONs are shown. This bonding scheme is to be compared to that of GM $MgTa_2B_6$ cluster as shown in Fig. 4.